JACC Vol. 27, No. 1
January 1996:161–72

New Method for Accurate Calculation of Regurgitant Flow Rate Based on Analysis of Doppler Color Flow Maps of the Proximal Flow Field

Validation in a Canine Model of Mitral Regurgitation With Initial Application in Patients

EHUD SCHWAMMENTHAL, MD, CHUNGUANG CHEN, MD, MARTIN GIESLER, MD,*
ALEX SAGIE, MD, J. LUIS GUERRERO, BS, JOSÉ ANTONIO VAZQUEZ DE PRADA, MD,
VINZENZ HOMBACH, MD,* ARTHUR E. WEYMAN, MD, FACC, ROBERT A. LEVINE, MD, FACC
Boston, Massachusetts and Ulm, Germany

Objectives. **The purpose of this study was to develop a rational and objective method for selecting a region in the proximal flow field where the hemispheric formula for calculating regurgitant flow rates by the flow convergence technique is most accurate.**

Background. **A major obstacle to clinical implementation of the proximal flow convergence method is that it assumes hemispheric isovelocity contours throughout the Doppler color flow map, whereas contour shape depends critically on location in the flow field.**

Methods. **Twenty mitral regurgitant flow rate stages were produced in six dogs by implanting grommet orifices into the anterior mitral leaflet and varying driving pressures so that actual peak flow rate could be determined from the known effective regurgitant orifice times the orifice velocity. Because plotting flow rate calculated by using a hemispheric formula versus alias velocities produces underestimation near the orifice and overestimation far from it, this plot was fitted to a polynomial function to allow identification of an inflection point within a relatively flat intermediate zone, where factors causing overestimation and underestimation are expected to be unimportant or balanced. The accuracy of flow rate calculation by the inflection point was compared with unselective and selective averaging techniques. Clinical relevance, initial feasibility and correlation with an independent measure were tested in 13 consecutive patients with mitral regurgitation who underwent cardiac catheterization.**

Results. **1) The accuracy of single-point calculations was improved by selecting points in the flat portion of the curve ($y = 1.15x - 3.34$, $r = 0.87$, SEE = 22.1 ml/s vs. $y = 1.34x - 1.99$, $r = 0.71$, SEE = 45.6 ml/s, $p < 0.01$). 2) Selective averaging of points in the flat portion of the curve further improved accuracy and decreased scatter compared with unselective averaging ($y = 1.08x + 4.8$, $r = 0.96$, SEE = 11.6 ml/s vs. $y = 1.30x + 0.6$, $r = 0.90$, SEE = 20.9 ml/s, $p < 0.01$). 3) The proposed algorithm for mathematically identifying the inflection point provided the best results ($y = 0.96x + 4.5$, $r = 0.96$, SEE = 9.9 ml/s), with a mean error of 1.6 ± 9.7 ml/s vs. 11.4 ± 11.7 ml/s for selective averaging ($p < 0.01$). In patients, the proposed algorithm identified an inflection point at which calculated regurgitant volume agreed best with invasive measurements ($y = 1.1x - 0.61$, $r = 0.93$, SEE = 17 ml).**

Conclusions. **The accuracy of the proximal flow convergence method can be significantly improved by analyzing the flow field mathematically to identify the optimal isovelocity zone before using the hemispheric formula to calculate regurgitant flow rates. Because the proposed algorithm is objective, operator independent and, thus, suitable for automatization, it could provide the clinician with a powerful quantitative tool to assess valvular regurgitation.**

(J Am Coll Cardiol 1996;27:161–72)

Mitral regurgitation occurs in patients with virtually all acquired and congenital heart diseases (1–3). Its presence and severity have a critical impact on clinical decision-making (4–9), creating the need for accurate noninvasive measures. Doppler color flow mapping of regurgitant jet area depends importantly on instrument settings (10–15), driving pressure (15–18) and interactions with adjacent atrial walls (19,20), creating recent interest in the hydrodynamically better behaved (laminar) ventricular flow field proximal to the regurgitant orifice, which can be visualized by Doppler color flow mapping with less dependence on instrument factors (21–26).

Flow acceleration toward the orifice produces concentric isovelocity shells. By continuity (conservation of mass), flow through any of these shells must pass through the orifice. Currently, flow rate is calculated by assuming that all shells are roughly hemispheric, with radii measured from the color flow

From the Cardiac Ultrasound Laboratory, Massachusetts General Hospital and Department of Medicine, Harvard Medical School, Boston, Massachusetts; and *Department of Internal Medicine, Division of Cardiology, University of Ulm, Ulm, Germany. Dr. Schwammenthal was supported by a grant from the Deutsche Forschungsgemeinschaft, Bonn, Germany. Dr. Levine is an Established Investigator of the American Heart Association, Dallas, Texas. This study was supported in part by Grant HL53702 from the National Heart, Lung, and Blood Institute, National Institutes of Health, Bethesda, Maryland and by a grant from the American Heart Association, Dallas.

Manuscript received June 28, 1994; revised manuscript received July 21, 1995, accepted August 1, 1995.

Address for correspondence: Dr. Ehud Schwammenthal, Cardiac Ultrasound Laboratory, Massachusetts General Hospital, VBK 508, Boston, Massachusetts 02114.

0735-1097/96/$15.00
0735-1097(95)00428-9

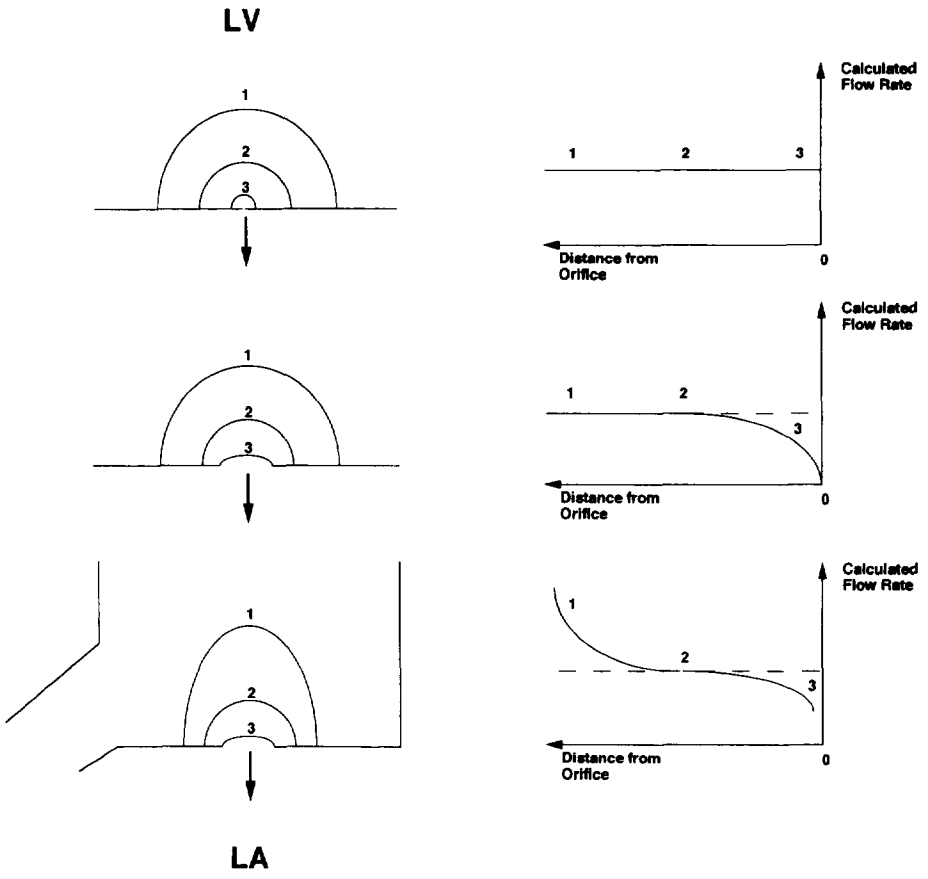

Figure 1. Schematic representation of isovelocity hemispheres proximal to a mitral regurgitant orifice as visualized by two-dimensional Doppler color flow mapping at three different distances (1, 2, 3) from the orifice **(left side)** and corresponding plots of calculated flow rates as a function of the distance from the orifice **(right side).** The **dashed lines** represent the actual regurgitant flow rate. Flow approaching a point orifice in a flat plate from infinity and without confinement by solid boundaries **(top)** will pass strictly hemispheric surfaces of decreasing area at an accelerating pace. Therefore, the regurgitant flow rate through any given isovelocity shell, calculated by using a hemispheric formula, will accurately reflect the orifice flow throughout the flow field. If flow approaches a *finite* orifice **(middle),** the isovelocity contour progressively flattens out, and use of a hemispheric formula to calculate flow will underestimate the true flow through the isovelocity shell close to the orifice (at high alias velocities) by underestimating its surface area. Confinement by solid boundaries, as well as the presence of the aortic outflow with its associated intraventricular flow field, increases the ratio of axial to transverse radius of the isovelocity shell far away from the orifice. The shape of the isovelocity shells therefore becomes increasingly "elliptic paraboloid," and a hemispheric formula will progressively overestimate the surface area of an isovelocity shell far away from the orifice (at low alias velocities), resulting in overestimation of flow **(bottom).** LA = left atrium; LV = left ventricle.

map (orifice to first alias point) and flow rate calculated as derived surface area × the alias velocity.

Although initial in vitro (22–24) and clinical results (27–33) have been encouraging, the hemispheric formula consistently produces underestimation at high alias velocities close to the regurgitant orifice (28) and significant overestimation at low alias velocities far from the regurgitant orifice (29). These observations are consistent with numeric solutions of the Navier-Stokes equations that show that the shape of the isovelocity shell critically depends on its location within the proximal flow field (34–38). This variable accuracy poses a serious problem for clinical application of an otherwise promising method.

The purpose of this study, therefore, was to develop a rational and objective method of selecting a region in the proximal flow field where the hemispheric formula for calculating regurgitant flow rate is most accurate, to promote clinical implementation of an accurate noninvasive tool.

Theoretic Background

Idealized inviscid flow approaching a point orifice in a flat plate without confining solid boundaries will form strictly hemispheric surfaces of increasing velocity (Fig. 1, top left). Calculated regurgitant flow rate Q_c through any isovelocity shell is then $Q_c = 2\pi r^2 \times V_a$ (where r is the radius of the hemispheric shell and V_a is the alias velocity), and the plot of flow rate calculated by this formula versus distance from the orifice is a horizontal line (Fig. 1, top right), as is the plot of flow rate versus alias velocity (a function of distance).

In reality, as flow approaches an orifice of *finite* size, the isovelocity contours progressively flatten out (36) (Fig. 1, middle left); the radius along the axis of flow becomes shorter than the transverse radius, so the hemispheric formula will underestimate surface area and flow rate (Fig. 1, middle right). This underestimation can be minimized by reducing the alias velocity to calculate Q_c far from the

orifice, if flow can approach equally from all directions (36,39).

In reality, however, with increasing distance from the orifice, the axial radius increases substantially relative to the transverse radius because of confinement by solid boundaries, which limit lateral access to the orifice (40,41) (Fig. 1, bottom left). This effect, magnified by interaction with the ventricular flow field associated with aortic outflow (42), produces increasingly elongated ("elliptic paraboloid" [38]) isovelocity shells; thus, a hemispheric formula will progressively overestimate surface area and flow rate (Fig. 1, bottom right), particularly as higher flow rates pass through the same chamber.

Mathematic formulation of the hypothesis. The plot of flow rate Q_c versus alias velocity V_a will therefore show underestimation near the orifice and overestimation far from it. This behavior is best represented by a polynomial function of the third order (see later), with an intermediate zone parallel (or almost parallel) to the x axis (Fig. 1, top) (42,43), where flow rate calculations employing a hemispheric formula will yield the closest estimates of true flow (isovelocity shells most nearly hemispheric). In particular, the curve is flattest exactly where its slope is minimal, that is, where its second derivative equals 0 (inflection point) (see Appendix). Therefore, we can propose the hypothesis that true (peak) regurgitant flow rate can be most closely and objectively estimated by obtaining the polynomial equation that describes calculated flow rate as a function of alias velocity, and then calculating the flow rate at which its second derivative is 0 (compare Appendix).

Methods

Animal preparation. The study conformed to the "position of the American Heart Association on Research Animal Use" adopted by the Association in 1984. Six adult dogs (25 to 35 kg) were anesthetized with sodium pentobarbital, 30 mg/kg body weight intravenously, intubated, and ventilated, with concentration of inspired oxygen and ventilation rate adjusted to keep blood gases at physiologic levels.

A left thoracotomy was performed, the pericardium was opened and calibrated micromanometer-tipped catheters (Millar Instruments) were used to record left ventricular, left atrial and central aortic pressures continuously with an electrocardiographic (ECG) lead (100-mm/s paper speed when data for each stage were formally recorded).

To control cardiac output, all venous return was drained from the superior and inferior venae cavae and coronary sinus and the filtered and oxygenated blood was returned to the right atrium through a wide bore cannula by a calibrated roller pump. Blood could also be pumped into or removed from the systemic arterial circuit through femoral cannulas to control left ventricular pressure independent of preload (44).

Mitral regurgitation was created under total cardiopulmonary bypass as previously reported (45,46). A plastic grommet (fixed orifice) with an internal diameter of 1.9 to 6.5 mm was inserted into the anterior mitral leaflet between its midportion and tip. The actual peak mitral regurgitant flow rate (Q_0) could thus be determined as effective orifice area × peak velocity (38). Effective orifice area was determined separately in vitro as the ratio of flow rate (measured with a stopwatch and graduated cylinder) and orifice velocity (38,47); it ranged from 2.6 to 25.2 mm^2. For the grommets studied the coefficient of contraction (effective/anatomic orifice area) ranged from 0.75 to 0.90. In two of the six dogs it was possible to replace a smaller grommet with a larger one under total cardiopulmonary bypass after the former had been used to complete an experimental series. Thus, a total of eight grommets could be studied in six dogs. Doppler color flow mapping was used to confirm the absence of additional sites of mitral regurgitation.

Experimental protocol. Arterial pressure was changed by varying roller pump flow into or out of the femoral artery at various levels of cardiac output (controlled by the flow pumped into the right atrium) and, thus, different levels of preload (end-diastolic pressure and cavity size). Dobutamine (20 μg/kg per min) was infused in three dogs to include hemodynamic states with small, hypercontractile left ventricles. A total of 20 stable stages (3 stages in four dogs, 4 stages in two dogs) covering a wide range of hemodynamic situations was thereby obtained with systolic arterial pressures of 40 to 140 mm Hg, left ventricular end-diastolic pressures of 2 to 35 mm Hg, left ventricular end-diastolic cavity diameters of 2.4 to 4.4 cm, cardiac outputs of 0.3 to 1.8 liters/min, heart rates of 80 to 110 beats/min and mean left atrial pressures of 4 to 35 mm Hg. In each experimental stage, continuous wave Doppler velocity interrogation and Doppler color flow mapping were performed while pressure recordings were constantly monitored to ensure hemodynamic stability during data collection.

Doppler echocardiography. The heart was stabilized in a pericardial cradle. Continuous wave Doppler and color flow mapping studies were performed with a commercially available system (Hewlett-Packard Sonos 1500) with a 2.5-MHz transducer. Mitral regurgitant velocities were obtained from an apical approach with the continuous wave Doppler beam aligned as parallel as possible to the mitral regurgitant jet to provide the most clearly delineated velocity envelopes.

Doppler color gain was adjusted to maximize signal without introducing spurious velocities in areas without flow. The lowest color wall filter possible was chosen and remained unchanged for all studies (48). Flow mapping was performed by using the shallowest depth and narrow sector angle capable of encompassing the proximal flow convergence region, orifice and proximal jet, with the transducer adjusted to provide optimal alignment between the ultrasound beam and the axial direction of flow. The magnification function was used to facilitate measurement of the flow convergence radius. Pulse repetition frequency was typically between 3.8 and 4.6 kHz. Velocity of flow (represented by color brightness) was measurable unambiguously up to 105 cm/s at a depth of 8 cm, up to 90 cm/s at 10 cm and up to 77 cm/s at 12 cm (Nyquists); the resulting frame rates were 33, 29 and 26 Hz, respectively.

With the use of ECG-gated triggering, color Doppler images at the time of the maximal extension of the proximal

flow field were acquired and frozen. Because of the processing delay between continuous wave and color Doppler images, this was achieved by adjusting the ECG trigger delay in the vicinity of the timing of peak continuous wave Doppler velocity to find the maximal extension, which for a fixed orifice truly corresponds to peak orifice velocity and flow. The machine then displayed a color-coded representation of the peak systolic flow velocity field proximal to the orifice, contained digitally in its memory. The distance from the orifice at which any given velocity occurred could be determined visually by shifting the alias velocity at which the color display changed from blue to red. This was done systematically by zero-shifting the baseline of the color Doppler scale on the frozen image (Fig. 2) from the lowest alias velocity available in the periphery of the flow field (which is not totally merged with ventricular outflow and thus is measurable) to the highest velocity close to the orifice (until no measurable isovelocity shell is displayed). In 2 of 20 stages regurgitant flow rate was too low to obtain the 8 to 10 data points typically available from one frozen image; in these two cases the Nyquist limit was changed to obtain additional alias cutoffs. The resulting alias velocities ranged from 11 to 81 cm/s. For each alias velocity three measurements of the axial radius of the isovelocity shell, from its zenith to the orifice, were averaged.

Data analysis. True flow rate was estimated by using the algorithm outlined under Theoretic Background. For each stage the surface area of all isovelocity shells visualized by systematic zero-shifting of the alias velocity was calculated by employing a hemispheric formula ($2\pi r^2$) and multiplied by the corresponding alias velocity V_a to calculate flow rate Q_c; Q_c was then plotted against V_a (Fig. 3, top). On the basis of a best-fit functional regression analysis (RS/1, release 4.3, BBN Software Products), a third-order polynomial function was used to relate Q_c and V_a. The first and second derivatives of Q_c with respect to V_a were also plotted as a function of V_a (Fig. 3, middle and bottom). True regurgitant flow rate Q_0 was then estimated as Q_c^* by solving the third-order polynomial function for an alias velocity at which its second derivative was equal to 0 (minimal slope: most nearly flat portion of the curve).

In addition, flow rate estimation was also performed for each stage by averaging all calculated flow rates at all alias velocities (unselective averaging) and by averaging only those calculated flow rates that appeared to lie in the flat portion of the graph between steepest ascents and declines (selective averaging).

Statistical analysis. Least-squares linear regression analysis was used to compare calculated and actual regurgitant flow rates. Differences between two regressions were tested for significance by using the F test. Because a wide range of values may yield a high correlation coefficient even when data are in poor agreement, we also determined the mean difference between pairs of flow rate estimates and actual values according to Bland and Altman (49), testing for significant differences between them by using a paired two-sample *t* test. To test the impact of orifice velocity, orifice size, regurgitant flow rate,

Figure 2. Example of the effect of selected alias velocity on size and shape of isovelocity shells as visualized by Doppler color flow mapping. Progressive baseline shifting of the alias limit was performed on frozen images. At the lowest alias velocity **(top)**, the isovelocity shell is elliptic paraboloid (high ratio of axial to lateral radius); at an intermediate alias velocity **(middle)**, the axial and lateral radii appear more even; and at high alias velocities **(bottom)**, the isovelocity shell is flat (low ratio of axial to lateral radius).

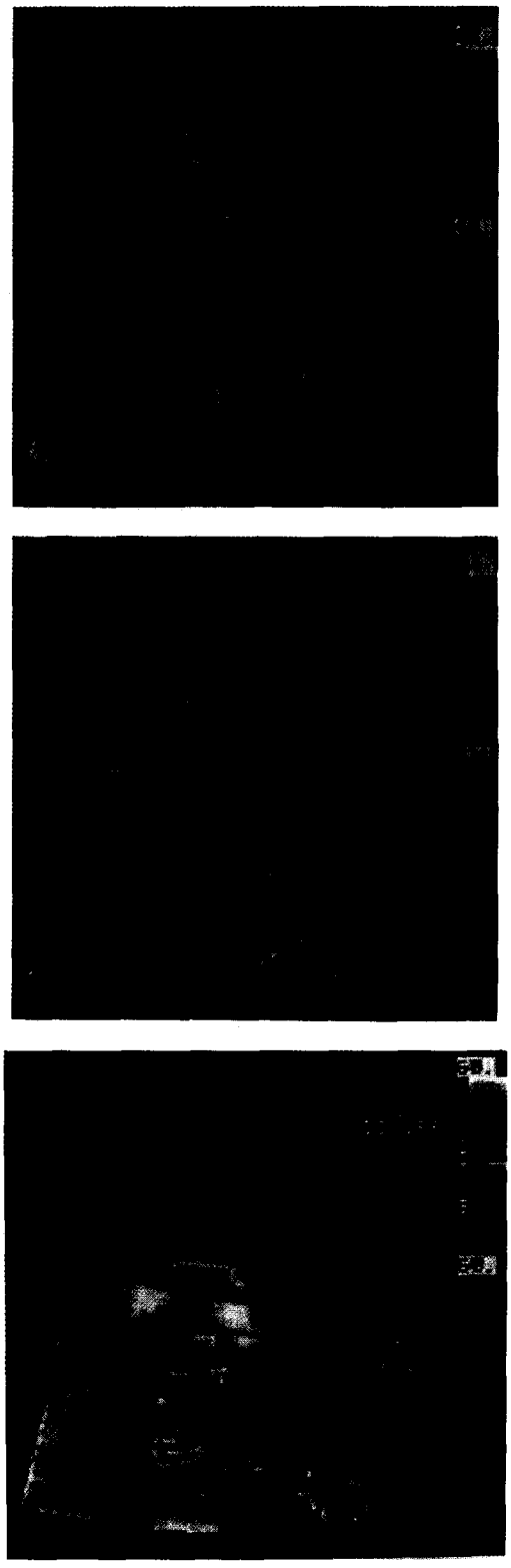

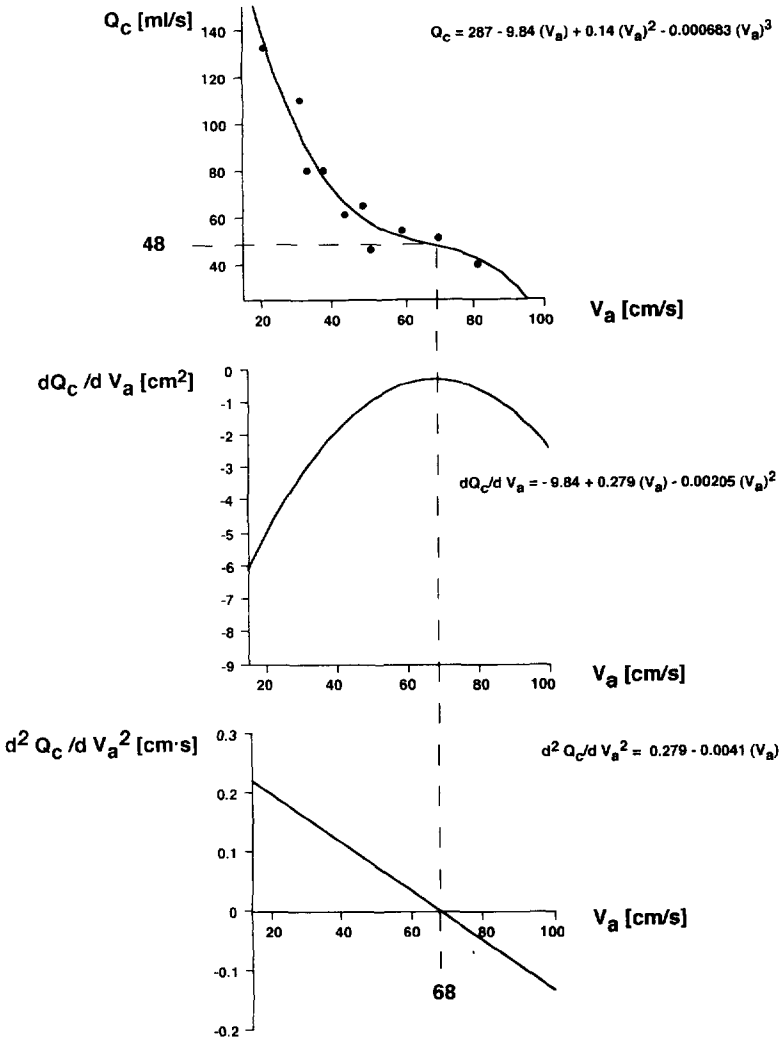

Figure 3. Plot of calculated flow rate Q_c (y axis) against the corresponding alias velocity V_a (x axis) **(top)** for an experimental stage. On the basis of a best fit analysis, a third-order polynomial function was used to express the relation between Q_c and V_a. The first derivative of Q_c with respect to V_a ($[dQ_c/dQ_a]$ yielding a second-order polynomial function) was obtained and plotted as a function of V_a **(middle)**. The second derivative of Q_c with respect to V_a ($[d^2Q_c/dV_a^2]$ yielding a linear function) was also obtained and plotted as a function of V_a **(bottom)**. The curve expressing the relation between Q_c and V_a **(top)** is flattest where the curve of the first derivative **(middle)** comes closest to 0 (i.e., at its optimum), which is exactly where the linear function of the second derivative **(bottom)** crosses 0. True regurgitant flow Q_0 was then estimated by solving the third-order polynomial function **(top)** for a V_a that yielded 0 when substituted in the linear function **(bottom)**. In this example, V_a was 68 cm/s, and solving the third-order polynomial function for this value yielded a flow rate of 48 ml/s. Actual regurgitant flow rate was 46 ml/s for this stage.

cardiac output and animal on the accuracy of the proposed method, we performed a stepwise multiple regression analysis, entering all of these factors as independent variables and the error of flow rate calculation as the dependent variable. The potential contribution of the individual variables was also tested by univariate analysis.

Variability of measurements was defined as the standard deviation of the differences between measurements. Intraobserver variability was tested by having one observer repeat the same measurements 10 days after the first measurements. Interobserver variability was tested by having two observers independently measure the same selected images. Intraobserver variability for radius measurements was 3.3%, with an interobserver variability of 5.7%, resulting in an interobserver variability of 1.0 ± 7.0 ml/s (9.5%) for algorithm-derived flow rates.

Patient studies. To test clinical relevance, initial feasibility and correlation with an independent invasive measure of regurgitation, we studied 13 consecutive patients (41 to 70 years old) with mitral regurgitation who underwent cardiac catheterization. Five had rheumatic valve disease, one had a history of infective endocarditis, five had functional mitral regurgitation due to ventricular dilation and two had mitral valve prolapse. Seven had sinus rhythm; six had atrial fibrillation.

All patients were studied by Doppler color flow mapping <6 h before catheterization with the use of an ATL Ultramark system (3-MHz phased array transducer and 2.25-MHz continuous wave Doppler echocardiograph). Examinations were performed from an apical window at the shallowest depth and narrowest sector angle to maximize frame rate (typically >20 Hz) at the lowest possible wall filter. The midsystolic frame showing the maximal extension of the proximal flow field was selected and frozen. Systematic baseline shifting (9 to 107 cm/s; higher maximal alias velocities permitted by higher flow rates) was performed as detailed earlier for three beats, which were averaged (during atrial fibrillation three beats with a cycle length corresponding to the mean). Peak midsystolic regurgitant flow rate was calculated by using the proposed algorithm and was normalized over the duration of the regurgitant period as Stroke volume = Peak regurgitant flow rate × Time-velocity integral/Peak orifice velocity by continuous wave Doppler study (28).

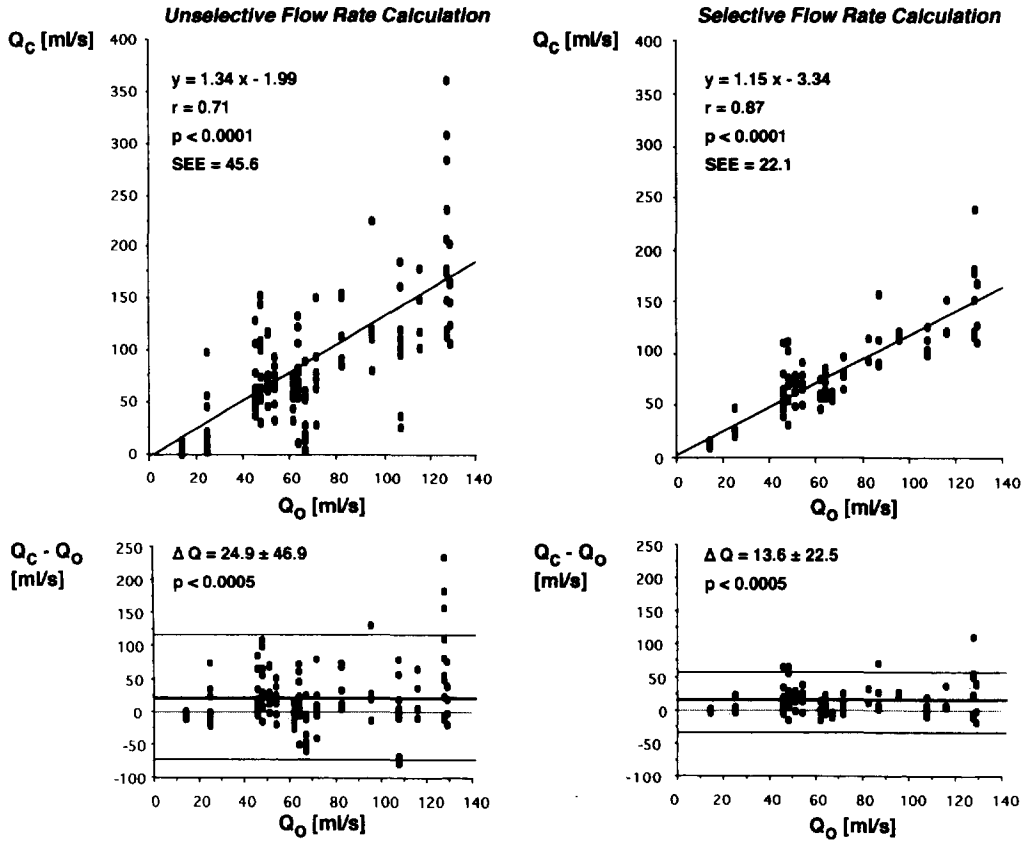

Figure 4. Comparison between unselective (**left**) and selective (**right**) single-point flow rate calculations (Q_c) using the proximal flow convergence method. **Top,** Correlation with actual regurgitant flow rates (Q_0) by linear regression analysis. **Bottom,** Mean difference (**thick line**) plotted together with the 95% confidence interval (**thin lines above and below zero level**). $\Delta Q = Q_c - Q_0$ = difference between calculated and actual flow rates.

Biplane left cineventriculography was performed (30° right and 60° left anterior oblique projection) with the injection of 40 to 45 ml of contrast agent at 18 ml/s. Mitral regurgitant stroke volume was determined as Angiographic (total) − Fick (effective) stroke volume, with the use of an average of three beats in patients with atrial fibrillation.

Results

Unselective and selective single-point flow rate calculations. Peak regurgitant flow rates ranged from 14 to 137 ml/s (mean 79 ± 35). Figure 4 (left) compares regurgitant flow rate calculated at *any* available alias velocity with actual regurgitant flow rate. Correlation was only fair, with substantial scatter (r = 0.71, SEE = 45.6 ml/s); the mean error (mean difference) was 24.9 ± 46.9 ml/s ($p < 0.0005$). Figure 4 (right) compares regurgitant flow rates calculated only in the relatively flat portion of the graph with actual regurgitant flow rates. Correlation was good (r = 0.87, SEE = 22.1 ml/s) and the amount of scatter significantly lower (F value 4.26, $p < 0.01$) than that obtained with unselective calculations, but there was still significant overestimation (mean error 13.6 ± 22.5 ml/s, $p < 0.0005$).

Unselective and selective averaging techniques. Unselectively averaging calculated flow rates at any available alias velocity for each stage (Fig. 5, left) yielded a good correlation with actual values (r = 0.90), but important scatter (SEE = 20.9 ml/s) and significant overestimation occurred, with a mean error of 18.7 ± 21.8 ml/s ($p < 0.0005$). Selectively averaging only those flow rate calculations in the flat portion of the graph (Fig. 5, right) significantly decreased both the degree of overestimation and the amount of scatter (r = 0.96, SEE = 11.6 ml/s), giving a mean error (11.4 ± 11.7 ml/s) significantly lower than that obtained with unselective averaging (F value 3.23, $p < 0.01$).

Application of the algorithm for detecting optimal alias velocity. Flow rate estimation employing the proposed algorithm (Fig. 3) yielded an excellent correlation with actual flow rate (r = 0.96, SEE = 9.9 ml/s) (Fig. 6). The mean error was 1.6 ± 9.7 ml/s ($p < 0.01$ vs. selective averaging, not significantly different from 0); that is, although the scatter was not significantly less than that for selective averaging, no significant overestimation or underestimation was now observed. Goodness of fit analyses showed high correlations for all 20 stages (r = 0.93 − 0.99, median 0.99) with a low SEE (7.6 ± 6.2 ml/s). For the given chamber sizes used, the optimal alias velocity determined by this algorithm correlated directly with the actual

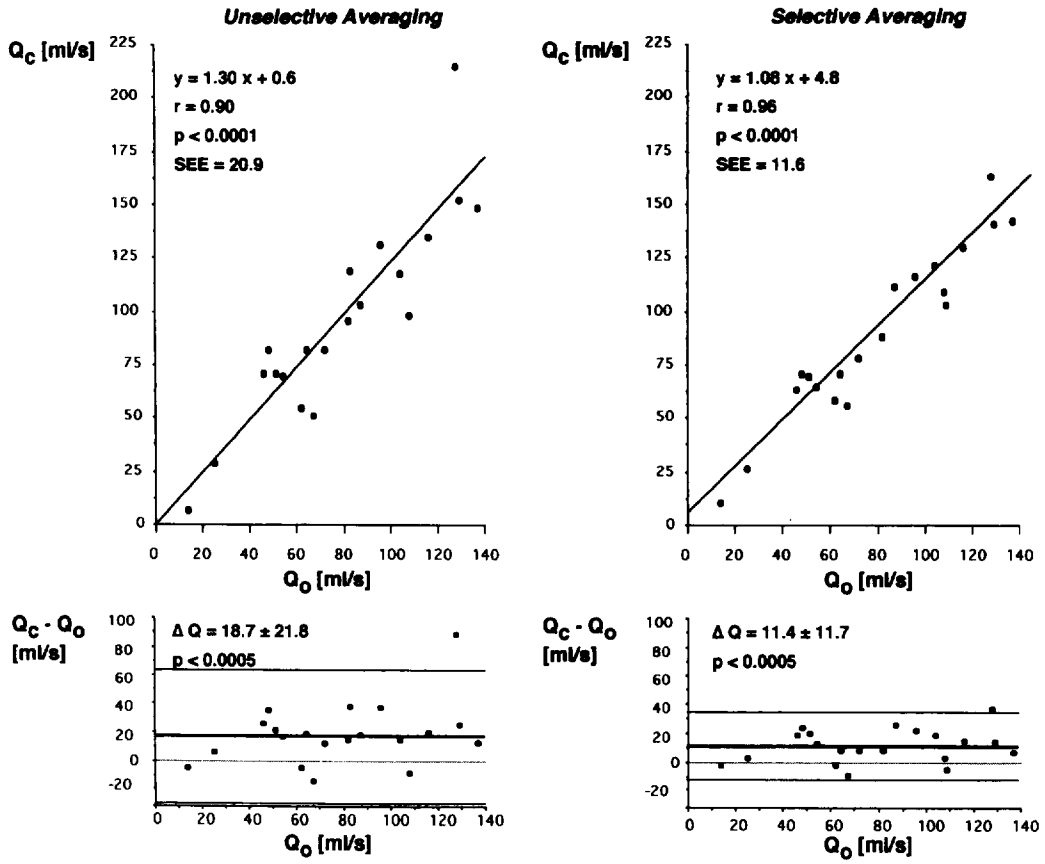

Figure 5. Comparison between unselective (**left**) and selective (**right**) averaging of flow rates (Q_c) calculated using the proximal flow convergence method. **Top,** Correlation with actual regurgitant flow rates (Q_0) by linear regression analysis. **Bottom,** Mean difference (**thick line**) plotted together with the 95% confidence interval (**thin lines above and below zero level**). $\Delta Q = Q_c - Q_0$ = difference between calculated and actual flow rates.

regurgitant flow rate (Fig. 7), whereas the radius (axial distance) at which flow rate calculation yielded optimal results was 4.9 ± 1.0 mm (95% confidence interval 2.9 to 5.9 mm), thus remaining within a relatively limited region. The percent error of flow rate calculation employing the algorithm was independent of orifice velocity, orifice size, actual regurgitant flow rate, cardiac output or animal ($p > 0.25$).

Patient studies. As in the canine model, applying the proposed algorithm allowed identification of an inflection point (Fig. 8, left) at which calculated volume flow agreed best with invasive measurements, with a correlation coefficient of 0.93. There was no systematic deviation of the line of regression from the line of identity ($y = 1.1x - 0.61$, SEE = 17 ml) (Fig. 8, right).

Discussion

Single aliasing techniques: variable geometry of proximal isovelocity shells. The present study demonstrates in vivo that the accuracy of flow rate calculations by the proximal flow convergence method critically depends on the alias velocity chosen, as the degree to which an isovelocity shell resembles a hemisphere varies with its location within the proximal flow field. If isovelocity shells are randomly selected and a hemispheric formula is used without relevant a priori considerations derived from theory (34–36,41) and experiment (37–40,42,43), systematic overestimation and considerable scatter result (Fig. 4, left). Although nonhemispheric models for surface area have been suggested (23), they require radial measurements from two orthogonal views, which are difficult to obtain in clinical practice.

Alternatively, plotting calculated regurgitant flow rate versus alias velocity and selecting data points in the relatively flat portion of this curve substantially reduced both scatter and the degree of systematic overestimation (Fig. 4, right). This approach simulates that of an experienced observer, who would consider *a priori* that underestimation occurs at very high alias velocities and overestimation at low alias velocities. However, selecting a single alias velocity for flow rate calculation remains arbitrary and subjective, thus necessarily introducing a source of scatter and variability, even when considering only data points from this flat zone. Moreover, in principle, because of converging flow not parallel to the Doppler beam, when the surface is truly a hemisphere it does not look like one, and vice versa.

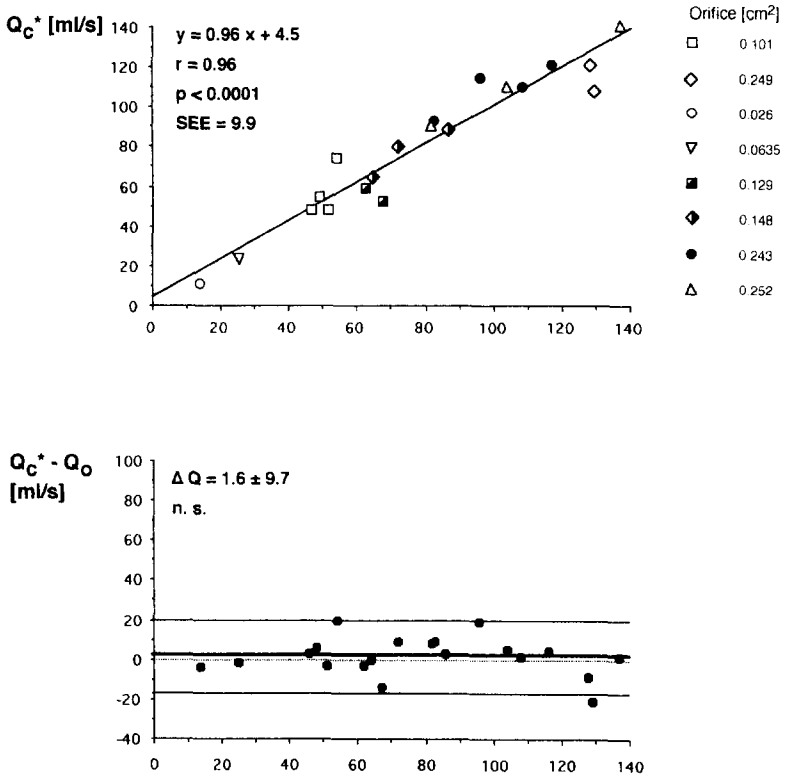

Figure 6. Correlation between flow rate calculation (Q_c^*) based on mathematic analysis of color Doppler flow maps of the proximal flow field using the proposed algorithm and actual regurgitant flow rates (Q_0). **Top,** Linear regression analysis. **Bottom,** Mean difference **(thick line)** plotted together with the 95% confidence interval **(thin lines above and below zero level).** $\Delta Q = Q_c - Q_0$ = difference between calculated and actual flow rates.

Multiple aliasing techniques: importance of the proximal velocity–radius relation. To overcome the problem of systematic overestimation or underestimation, it has been suggested (37,38) that flow rates calculated with different alias velocities should be averaged. Experimentally, Zhang et al. (38) substantially improved accuracy by averaging flow rate calculations from three alias boundaries, but significant overestimation remained, indicating a nonlinear relation between flow rate estimates and alias velocity, and it could not be remedied by linear averaging. Shandas et al. (37) proposed averaging flow rate calculations from multiple aliasing zones. In the present study such unselective averaging did not yield better results than a selective single alias technique. In contrast, *selective* averaging of flow rate calculations in the relatively flat portion of the curve yielded excellent substantial reduction in both scatter and the degree of overestimation. Although the current study is principally in agreement with those discussed (37,38), it addresses the question of how to select appropriate alias

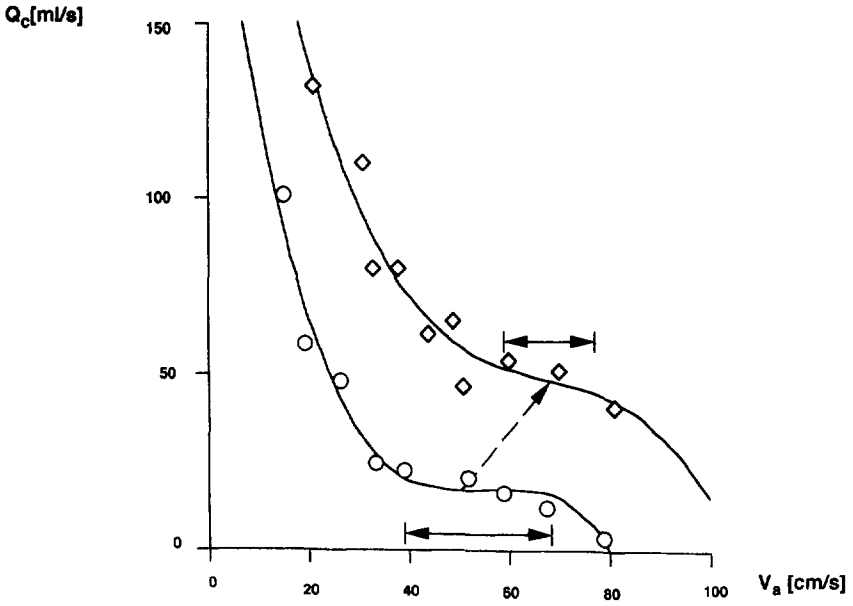

Figure 7. Plots of calculated flow rate Q_c (y axis) against the corresponding alias velocity V_a (x axis) for two different flow stages, showing variation in the range of isovelocity shells suitable for accurate calculation. The optimal alias velocity **(dashed arrow)** derived by the algorithm was higher at 48 ml/s **(diamonds)** than at 23 ml/s **(circles).** At a flow rate of 23 ml/s, there is a plateau spanning alias velocities from 39 to 68 cm/s, at which flow rate estimations yield accurate results **(arrows).** At a flow rate of 46 ml/s, there is no real plateau, only a flatter slope, limiting accurate flow rate estimation to values between 59 and 78 cm/s **(arrows).** The precise location of the optimal zone was not constant, and its width varied for different curves.

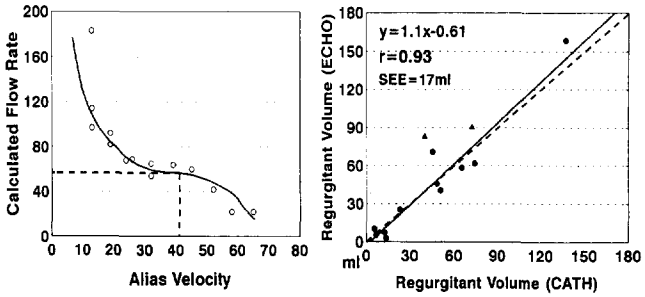

Figure 8. Left, Plot of calculated flow rate (y axis) against the corresponding alias velocity (x axis) for a patient with moderate mitral regurgitation. The **vertical dashed line** through the inflection point of the curve indicates the optimal alias velocity; the **horizontal dashed line** indicates the algorithm-derived estimate of regurgitant flow rate. **Right,** Correlation between invasively (cardiac catheterization [CATH]) and noninvasively (echocardiography [ECHO]) determined regurgitant stroke volumes in 13 patients with mitral regurgitation.

velocities for flow rate calculation: It first identifies the optimal alias zone by analysis of the Doppler flow map and then averages only flow rate calculations derived from that zone.

Hemispheric aliasing identifying algorithm. Although selective averaging can be readily applied without additional equipment, it would be desirable to take advantage of the full digital velocity map to calculate accurate regurgitant flow rate estimates automatically. Because this requires an operator-independent algorithm, we developed a method to identify the optimal alias velocity based on mathematic analysis of the velocity-radius relation within the proximal flow field. Instead of having an operator select points for averaging, a third-order polynomial function is fitted to the data set and solved for an alias velocity at which its slope is minimal (inflection point, second derivative = 0), identifying an isovelocity shell where the hemispheric formula works best. This optimal alias velocity increases with increasing flow rate (Fig. 7), although its distance from the orifice varies within a relatively limited zone (roughly 3 to 6 mm in the animals studied) away from the extremes of the flow field (36,38,40–43). Nevertheless, the precise location of this zone is not constant and its width varies for different curves (Fig. 7), emphasizing the need to identify this zone correctly for each curve, either by an analytic technique as in the present study or by a nomographic method as suggested by others (26,30,50,51).

This proposed algorithm has two important strengths: 1) Although flow rate is finally calculated at only one alias velocity, this point is derived by taking full advantage of the complete data set. The fitted curve from which flow rate is actually calculated will act to reduce the effect of measurement error in the raw data, thereby decreasing scatter in flow rate estimation. 2) Because the optimal alias velocity is identified from the fitted function, an actual data point need not be present exactly at the optimal alias velocity, whose location is initially unknown; the only precondition is that the sampled isovelocity shells span the inflection point. This should be the case, as in the present study, when going through a stepwise baseline-shifting process from the lowest alias velocity in the periphery of the flow field to the highest alias velocity close to the orifice, as visually confirmed during data collection (Fig. 2). Accuracy could be increased by entering more isovelocity shells into the analysis from a digitized flow map, which could also be combined with an orifice-localizing algorithm (52).

Rationale of curve fitting. Theoretic predictions from the Navier-Stokes equations, as well as experimental studies, have demonstrated that at least two major factors (confinement and finite orifice size) can independently determine the shape of an isovelocity shell for any given flow rate (25,34–42). Therefore, functions that allow only for one factor to influence the data curve (such as linear, square root, parabolic, hyperbolic or monoexponential functions) are not necessarily optimal. We therefore chose the most general approach, the Taylor series expansion, or, over a specific interval, the Weierstrass approximation theorem (53), which states that every function that is continuous in an interval over which its derivatives exist can be represented in that interval, to any desired degree of accuracy, by a polynomial. The theoretic justification for a polynomial is, therefore, its ability to express any data set that is influenced by several independent factors and thus has zones of different slope (for example, progressive overestimation, progressive underestimation and a flatter slope in between). The order of the polynomial must be guided by empiric factors, in particular the signal to noise ratio (radius measurement error) and the number of data points. A high order polynomial function will tend to fit the noise rather than the data. A lower order polynomial function will therefore be more robust, with the third order representing the minimal order polynomial still capable of showing slope inflections. In fact, in each of the 20 stages analyzed, over a wide range of flow rates, a third-order polynomial function provided a highly accurate fit, with only 2 stages where a fourth-order and fifth-order polynomial would have fit equally well. Although we do not propose that a third-order polynomial always provides the best fit, a polynomial fit of some order will always be able to fit the data to any desired degree, in order to derive an optimal flow rate estimation. Nevertheless, use of a third-order polynomial in this study yielded highly accurate results.

Quantification of mitral regurgitation in the clinical setting. The algorithm could be successfully applied in the initial series of patients studied, demonstrating clinical relevance, feasibility and good correlation with quantitative angiography. As expected, scatter was greater than for the ideal experimental setting, with potential contributing factors that include 1) the well known variability of the invasive technique (54) with inherent propagation of error from subtracting two large numbers; 2) nonsimultaneity of invasive and noninvasive measurements (difficulty in performing careful color flow mapping on the catheterization table); and 3) the variability induced by the currently implemented method for translating a midsystolic regurgitant flow rate into regurgitant stroke volume.

The ideal method for taking pulsatile variation into account

would be to apply an optimal alias velocity algorithm to multiple frames obtained with high temporal resolution color flow mapping, or to multiple color M-mode lines, neither of which is currently available on standard echocardiographic equipment. As a clinically convenient alternative we chose for this initial series the continuous wave Doppler technique, which accounts for changes only in driving pressure, not orifice area. The observation that the two patients with late systolic mitral valve prolapse (triangles, Fig. 8, right), and thus phasic variation of orifice area, demonstrated significant overestimation is consistent with this limitation.

Moreover, peak regurgitant flow rate itself has been shown to be quite useful in separating angiographic degrees of mitral regurgitation (27). Finally, it was not the purpose of this study to address the ongoing question of temporal correction, but rather to provide an accurate method of peak flow rate estimation, which is the prerequisite for any accurate proximal flow convergence technique.

Limitations of the study. Actual regurgitant flow rates were determined by using a highly accurate reference standard: multiplying the effective orifice area of a grommet, measured in vitro, by the peak orifice velocity, which can be measured with high precision by continuous wave Doppler echocardiography. This method is highly accurate compared with measurements of center stream velocities by laser Doppler anemometry (55,56), the engineering reference standard (57,58). This grommet model has also been validated for providing highly accurate measurements not only of the pressure gradient, but even of the rate of change of pressure (dP/dt) and the time constant of isovolumetric relaxation (45,46). It takes advantage of the basic concept behind orifice meters, commonly used in mechanical engineering to measure flow rates in pipes (59), and has also been used to calibrate mitral regurgitant flow rates in another in vivo model (38). A round, flat grommet, however, may not be representative of the full range of clinically observed regurgitant orifices with complex local and global geometry (41,60) and temporal variation (61,62); if important clinically, however, these factors can be accounted for by proposed modifications (29,63). Variation of the coefficient of contraction, although not observed in vivo (61), should not affect the results of the present study for several reasons: 1) Flow rate was measured *at one point* during the cardiac cycle; 2) the coefficient of contraction was determined for the same hemodynamic setting (driving pressure as in vivo), as done by Zhang et al. (38); and 3) the proximal flow convergence method assesses flow and, when combined with orifice velocity measurements, can be used to determine effective regurgitant orifice area directly, without knowledge of the coefficient of contraction.

Clinical implications. Despite the promising initial results of the proximal flow convergence method, the major obstacle to its application has been uncertainty regarding the location of measurement that would provide the most accurate results. This study has demonstrated that this uncertainty can be removed by first analyzing the flow field to identify the optimal isovelocity zone before employing the hemispheric formula for calculating regurgitant flow rate. At the same time, automatization of the proposed algorithm and incorporation into current echocardiographic equipment could avoid time-consuming off-line analyses, to keep the method attractive for daily clinical application. The improved accuracy of the proximal flow convergence method, combined with the objectivity of the algorithm, would constitute an important advantage for clinical decision-making and guidance of medical and surgical therapy.

Appendix

The relation between calculated flow rate (y) and alias velocity (x) is expressed as a third-order polynomial function:

$$y = f(x) = a_3x^3 + a_2x^2 + a_1x + a_0, \quad [1]$$

where f(x) is the functional relation between x and y defined by the polynomial coefficients a_0 to a_3. To determine where the graph runs parallel (or almost parallel) to the x axis we must find where its slope (first derivative) is minimal, which occurs where its second derivative equals 0 (the inflection point):

$$y'' = f''(x) = d^2x/dy^2 = 6a_3x + 2a_2 = 0, \quad [2]$$

where y'', f''(x) and d^2x/dy^2 all refer to the second derivative of the polynomial relation with respect to x. Hence, true regurgitant flow can be most closely estimated by solving the polynomial function y = f(x) for an alias velocity [x], which yields 0 when substituted in y'' = f''(x) (see Fig. 3).

References

1. Levy MJ, Edwards JE. Anatomy of mitral insufficiency. Prog Cardiovasc Dis 1962;5:119–44.
2. Silverman ME, Hurst JW. The mitral complex. Interaction of the anatomy, physiology and pathology of the mitral annulus, mitral valve leaflets, chordae tendineae, and papillary muscles. Am Heart J 1968;76:399–418.
3. Perloff JK, Roberts WC. The mitral apparatus. Functional anatomy of mitral regurgitation. Circulation 1972;46:227–37.
4. Barzilai B, Davis VG, Stone PH, Jaffe AS, and the MILIS Study Group. Prognostic significance of mitral regurgitation in acute myocardial infarction. Am J Cardiol 1990;65:1169–75.
5. Lehman KG, Francis MD, Dodge HT, and the TIMI Study Group. Mitral regurgitation in early myocardial infarction. Ann Intern Med 1992;117:10–7.
6. Galloway AC, Colvin SB, Baumann FG, Harty S, Spencer FC. Current concepts of mitral valve reconstruction for mitral insufficiency. Circulation 1988;78:1087–98.
7. Zile MR. Chronic aortic and mitral regurgitation: choosing the optimal time for surgical correction. Cardiol Clin 1991;9:239–53.
8. Maurer G, Czer LSC, Chaux A, et al. Intraoperative Doppler color flow mapping for assessment of valve repair for mitral regurgitation. Am J Cardiol 1987;60:333–7.
9. Stewart WJ, Currie PJ, Salcedo EE, et al. Intraoperative Doppler color flow mapping for decision-making in valve repair for mitral regurgitation: technique and results in 100 patients. Circulation 1990;81:556–66.
10. Utsunomiya T, Ogawa T, King SW, et al. Pitfalls in the display of Doppler color jet areas: combined variability due to Doppler angle, frame rate and scanning direction. Echocardiography 1990;7:739–45.
11. Stewart WJ, Cohen GI, Salcedo EE. Doppler color flow image size: dependence on instrument settings. Echocardiography 1991;8:319–27.
12. Sahn DJ. Instrumentation and physical factors related to visualization of stenotic and regurgitant jets by Doppler color flow mapping. J Am Coll Cardiol 1988;12:1354–65.

13. Hoit BD, Jones M, Eidbo EE, Elias W, Sahn DJ. Sources of variability for Doppler color flow mapping of regurgitant jets in an animal model of mitral regurgitation. J Am Coll Cardiol 1989;13:106–15.
14. Cape EG, Yoganathan AP, Levine RA. Increased heart rate can cause underestimation of regurgitant jet size by Doppler color flow mapping. J Am Coll Cardiol 1991;21:1029–37.
15. Bolger AF, Eigler NL, Pfaff JM, Resser KJ, Maurer G. Computer analysis of Doppler color flow mapping images for quantitative assessment of in vitro fluid jets. J Am Coll Cardiol 1988;12:450–7.
16. Simpson IA, Valdes-Cruz LM, Sahn DJ, Murillo A, Tamura T, Chung KY. Doppler color flow mapping of simulated in vitro regurgitant jets: evaluation of the effects of orifice size and hemodynamic variables. J Am Coll Cardiol 1989;13:1195–207.
17. Cape EG, Skoufis EG, Weyman AE, Yoganathan AP, Levine RA. A new method for noninvasive quantification of valvular regurgitation based on conservation of momentum. In vitro validation. Circulation 1989;79:1343–53.
18. Thomas JD, Liu CM, Flachskampf FA, O'Shea JP, Davidoff R, Weyman AE. Quantification of jet flow by momentum analysis: an in vitro color Doppler flow study. Circulation 1990;81:247–59.
19. Cape EG, Yoganathan AP, Weyman AE, Levine RA. Adjacent solid boundaries alter the size of regurgitant jets on Doppler color flow maps. J Am Coll Cardiol 1991;17:1094–102.
20. Chen C, Thomas JD, Anconina J, et al. Impact of impinging wall jet on color Doppler quantification of mitral regurgitation. Circulation 1991;84:712–20.
21. Simpson IA, Sahn DJ, Valdes-Cruz LM, Chung KJ, Sherman FS, Swensson RE. Color Doppler flow mapping in patients with coarctation of the aorta: new observations and improved evaluation with color flow diameter and proximal acceleration as a predictor of severity. Circulation 1988;77:736–44.
22. Recusani F, Bargiggia GS, Yoganathan AP, et al. A new method for quantification of regurgitant flow rate using color flow imaging of the flow convergence region proximal to a discrete orifice: an in vitro study. Circulation 1991;83:594–604.
23. Utsunomiya T, Ogawa T, Doshi R, et al. Doppler color flow "proximal isovelocity surface area" method for estimating volume flow rate: effects of orifice shape and machine factors. J Am Coll Cardiol 1991;17:1103–11.
24. Utsunomiya T, Ogawa T, Tang HA, et al. Doppler color flow mapping of the proximal isovelocity surface area: a new method for measuring volume flow rate across a narrowed orifice. J Am Soc Echocardiogr 1991;4:338–48.
25. Shandas R, Gharib M, Liepmann D, Shiota T, Sahn DJ. Experimental studies to define the geometry of the flow convergence region: laser Doppler particle tracking and color Doppler imaging. Echocardiography 1992;9:43–50.
26. Giesler MO, Stauch M. Color Doppler determination of regurgitant flow: from proximal isovelocity surface areas to proximal velocity profiles. An in vitro study. Echocardiography 1992;9:51–62.
27. Bargiggia GS, Tronconi L, Sahn DJ, et al. A new method for quantification of mitral regurgitation based on color flow Doppler imaging of flow convergence proximal to regurgitant orifice. Circulation 1991;84:1481–9.
28. Rivera JM, Vandervoort P, Thoreau D, et al. Quantification of mitral regurgitation with the proximal flow convergence method: a clinical study. Am Heart J 1992;124:1289–96.
29. Chen C, Koschyk D, Brockhoff C, et al. Noninvasive estimation of regurgitant flow rate and volume in patients with mitral regurgitation by color Doppler mapping of accelerating flow field. J Am Coll Cardiol 1993;21:374–83.
30. Utsunomiya T, Nguyen D, Rajen D, Patel D, Gardin JM. Regurgitant volume estimation in mitral regurgitation by color Doppler using the "proximal isovelocity surface area" method [abstract]. Circulation 1989;80 Suppl II:II-577.
31. Xie GY, Berk MR, Smith MD, Hixson CS, Harrison MR, DeMaria AN. Quantification of mitral regurgitant volume using color Doppler PISA method—a clinical study [abstract]. J Am Coll Cardiol 1992;19 Suppl A:379A.
32. Yoshida K, Yoshikawa J, Akasaka T, Nishigami K, Minagoe S. Value of acceleration flow signals proximal to the leaking orifice in assessing the severity of prosthetic mitral valve regurgitation. J Am Coll Cardiol 1992;19:333–8.
33. Giesler M, Grossman G, Schmidt A, et al. Color Doppler echocardiographic determination of mitral regurgitant flow from the proximal flow velocity profile of the flow convergence region. Am J Cardiol 1993;71:217–24.
34. Bommer W, Kacheria N. Finite difference analysis of regurgitant flow analysis lines: a Navier-Stokes solution to quantitate regurgitant flow [abstract]. Circulation 1990;82 Suppl III:III-552.
35. Barclay SA, Eidenvall L, Karlson M, et al. The shape of the proximal isovelocity surface area varies with regurgitant orifice size and distance from orifice: computer simulation and model experiments with color M-mode technique. J Am Soc Echocardiogr 1993;6:433–45.
36. Rodriguez L, Anconina J, Flachskampf FA, Weyman AE, Levine RA, Thomas JD. Impact of finite orifice size on proximal flow convergence. Implications for Doppler quantification of valvular regurgitation. Circ Res 1992;70:923–30.
37. Shandas R, Valdes-Cruz LM, Jones M, Izumi Y. The proximal flow convergence technique can be applied to complex physiological flows: animal studies of mitral regurgitation and stenosis using digital color Doppler [abstract]. Circulation 1992;86 Suppl I:I-805.
38. Zhang J, Jones M, Shandas R, et al. Accuracy of flow convergence estimates of mitral regurgitant flow rates obtained by use of multiple color flow Doppler M-mode aliasing boundaries: an experimental animal study. Am Heart J 1993;125:449–58.
39. Utsunomiya T, Doshi R, Patel D, et al. Calculation of volume flow rate by proximal isovelocity surface area method: simplified approach using color Doppler zero baseline shift. J Am Coll Cardiol 1993;22:277–82.
40. Liepmann D, Shandas R, Dommermuth D, Sahn DJ. Effect of adjacent boundary formation on the proximal flow convergence region: Comparison of color Doppler flow mapping with theoretical and gold standard velocity measurement techniques [abstract]. J Am Coll Cardiol 1993;21 Suppl A:298A.
41. Thomas JD, Powell KA, Greenberg N, Vandervoort PM, Stewart WJ. Use of proximal convergence method to quantitate mitral regurgitation in patients with a flail leaflet: Lessons from fluid dynamic modelling [abstract]. J Am Coll Cardiol 1993;21 Suppl A:458A.
42. Chen C, Vandervoort PM, Heik S, Weyman AE, Thomas JD. Is the proximal flow convergence method accurate in the presence of a second outflow? [abstract]. Circulation 1992;86 Suppl I:I-805.
43. Weintraub R, Shandas R, Cranney G, Walker P, Yoganathan AP, Sahn DJ. Comparison of flow convergence calculations using color Doppler flow mapping and phase velocity encoded MRI: an in-vitro study [abstract]. Circulation 1991;84 Suppl II:II-36.
44. Choong CY, Abascal VM, Thomas JD, Guerrero JL, McGlew S, Weyman AE. Combined influence of ventricular loading and relaxation on the transmitral flow velocity profile in dogs measured by Doppler echocardiography. Circulation 1988;78:672–83.
45. Chen C, Rodriguez L, Guerrero JL, et al. Noninvasive estimation of the instantaneous first derivative of left ventricular pressure using continuous-wave Doppler echocardiography. Circulation 1991;83:2101–10.
46. Chen C, Rodriguez L, Levine RA, Weyman AE, Thomas JD. Noninvasive measurement of the time constant of left ventricular relaxation using the continuous-wave Doppler velocity profile of mitral regurgitation. Circulation 1992;86:272–8.
47. Flachskampf FA, Weyman AE, Guerrero JL, Thomas JD. Influence of orifice geometry and flow rate on effective valve area: an in vitro study. J Am Coll Cardiol 1990;15:1173–80.
48. Vandervoort PM, Aghassi DS, Thoreau DH, et al. Wall motion filters introduce significant error in flow rate calculation by the proximal flow convergence method: theoretical analysis and in vitro study. J Am Soc Echocardiogr. In Press.
49. Bland JM, Altman DG. Statistical methods for assessing agreement between two methods of clinical measurement. Lancet 1986;1:307–10.
50. Shiota T, Teien D, Deng YB, et al. Estimation of regurgitant flow volume based on centerline velocity/distance profiles using color M-Q Doppler: application to orifices of different shapes. J Am Coll Cardiol 1994;24:440–5.
51. Shiota T, Jones M, Teien DE, et al. Evaluation of mitral regurgitation using a digitally determined color Doppler flow convergence "centerline" acceleration method: studies in an animal model with quantified mitral regurgitation. Circulation 1994;89:2879–87.
52. Vandervoort PM, Thoreau DH, Rivera JM, Levine RA, Weyman AE, Thomas JD. Automated flow rate calculations based on digital analysis of flow convergence proximal to regurgitant orifices. J Am Coll Cardiol 1993;22:535–41.
53. Kelly LG. Handbook of Numerical Methods and Applications. Reading (MA); Menlo Park (CA); London; Don Mills (Ontario, Canada); Addison-Wesley, 1967:10, 157, 321.
54. Croft CH, Lipscomb K, Mathis K, et al. Limitations of qualitative angiographic grading in aortic or mitral regurgitation. Am J Cardiol 1984;53:1593–8.

55. Valdes-Cruz LM, Yoganathan AP, Tamura T, Tomizuka F, Woo YR, Sahn DJ. Studies in vitro of the relationship between ultrasound and laser Doppler velocimetry and applicability of the simplified Bernoulli relationship. Circulation 1986;73:300–8.
56. von Bibra H, Stempfle HU, Poll A, Scherer M, Blüml G, Blömer H. Limitations of flow detection by color Doppler: in vitro comparison to conventional Doppler. Echocardiography 1991;8:633–42.
57. Yoganathan AP. Prosthetic heart valves: a study of in vitro performance, phase II, final report. Washington, D.C.: FDA; FDA contract 223-81-5000(NTIS No. PB 84-162387).
58. Yoganathan AP, Reamer HH, Corcoran WH, Harrison EC. A laser-Doppler anemometer to study velocity fields in the vicinity of prosthetic heart valves. Med Biol Eng Comput 1979;17:38.
59. Munson BR, Young DF, Okiishi TH. Fundamentals of Fluid Mechanics, New York: Wiley, 1990:135, 528.
60. Grayburn PA, Fehske W, Omran H, Brickner ME, Luderitz B. Multiplane transesophageal echocardiographic assessment of mitral regurgitation by Doppler color flow mapping of the vena contracta. Am J Cardiol 1994;74:912–7.
61. Yellin EL, Yoran C, Sonnenblick EH, Gabbay S, Frater RWM. Dynamic changes in the canine mitral regurgitant orifice area during ventricular ejection. Circ Res 1979:677–83.
62. Schwammenthal E, Chen C, Benning F, Block M, Breithardt G, Levine RA. Dynamics of mitral regurgitant flow and orifice area: physiologic application of the proximal flow convergence method. Clinical data and experimental testing. Circulation 1994;90:307–22.
63. Rodriguez L, Thomas JD, Monterroso V, et al. Validation of the proximal flow convergence method: calculation of orifice area in patients with mitral stenosis. Circulation 1993;88:1157–65.